Energy Generating Electronic Skin With Intrinsic Tactile Sensing Without Touch Sensors

Pablo Escobedo, Markellos Ntagios, Dhayalan Shakthivel, William T. Navaraj, and Ravinder Dahiya, *Fellow, IEEE*

***Abstract*—Electronic skin (eSkin) with various types of sensors over large conformable substrates has received considerable interest in robotics. The continuous operation of large number of sensors and the readout electronics make it challenging to meet the energy requirements of eSkin. In this article, we present the first energy generating eSkin with intrinsic tactile sensing without any touch sensor. The eSkin comprises a distributed array of miniaturized solar cells and infrared light emitting diodes (IRLEDs) on soft elastomeric substrate. By innovatively reading the variations in the energy output of the solar cells and IRLEDs, the eSkin could sense multiple parameters (proximity, object location, edge detection, etc.). As a proof of concept, the eSkin has been attached to a 3-D-printed hand. With an energy surplus of 383.6 mW from the palm area alone, the eSkin could generate more than 100 W if present over the whole body (area $\sim$1.5 m^2). Further, with an industrial robot arm, the presented eSkin is shown to enable safe human−robot interaction. The novel paradigm presented in this article for the development of a flexible eSkin extends the application of solar cell from energy generation alone to simultaneously acting as touch sensors.**

***Index Terms*—Electronic skin (eSkin), energy harvesting, human−robot interaction (HRI), proximity sensing, solar cell, touch sensing.**

I. Introduction

Electronic skin or "eSkin" has recently emerged as a novel platform for advances in robotics, prosthesis, health diagnostics, therapeutics, and monitoring [1]. It allows robots and prosthetic limbs to gather tactile information from large area contacts and to exploit the same to operate in unstructured environment or to improve human−robot interaction (HRI) [2]–[6]. Likewise, eSkin has been explored for measurement of vital health parameters and to provide reliable, effective, and, sometimes, life-saving functions [7]–[9]. With increasing number and type of sensors (pressure, temperature, texture, proximity, etc.) and electronics associated with them on large area eSkin [10]–[13], a stable power supply is critical for practical usage [11], [14]. Thus, a realistic and accessible power source is urgently needed for a next-generation of smart, stand-alone, always-on eSkins. This is a challenge as the continuous power supply through batteries is not practical because they add weight, are not flexible, and may require redesigning of robotics platform [15], [16]. Likewise, for applications requiring intimate integration of eSkin with human skin (e.g., health monitoring through tattoo-like patches) [17], the skin offers an extremely harsh environment for the power generation. Various attempts to address the energy issue have so far focused on either minimizing the use power through low-power electronics [18], [19] and event-driven approaches for tactile data readout from selected locations [20]–[24] or by using various types of energy harvesters [11], [15], [25]–[27]. To this end, we recently demonstrated an energy autonomous eSkin with graphene-based transparent touch sensing layer integrated on solar cells [28]. The touch sensitive layer in this work required ultra-low power ($\sim$20 nW/cm^2) for operation, and in a following work, we also showed that the excess energy generated by solar cells could be stored in flexible supercapacitors underneath to allow eSkin to function when there is no light [29], [30]. Nonetheless, this approach as well as other eSkin approaches reported in the literature [4] require separate touch sensitive and energy generating devices.

In this article, we present a new approach, whereby the eSkin does not have any touch sensitive layer or touch sensor. Instead, the energy generating device, i.e., photovoltaic (PV) or solar cell itself is used as the sensor. The solar cells generate energy when the light reaches their surface. This means whenever a solar cell is shadowed by an approaching object, the amount of generated energy will reduce from maximum to zero—with zero energy signifying the contact. This simple fact is exploited here to detect the proximity and the contact of an object in a robotic hand, while continuing to generate the energy. The new concept has been demonstrated through an array of solar cells integrated on a 3-D-printed robotic hand, as shown in Fig. 1. The sensing system consists of discrete Si PV cells integrated on soft and flexible polydimethylsiloxane (PDMS) substrate for conformable coverage of curved surfaces. The developed eSkin has two modes of operation: 1) shadow detection and 2) proximity sensing. The developed skin shows continuous power generation in the range of $\sim$10 mW/cm^2, considering the whole array of solar cells distributed in the palm area. Unlike traditional power-hungry eSkins, the unique architecture presented here demonstrates a power-surplus or power-generating eSkin. The approach presented here also shows that, when it comes to engineered solution, the distribution of sensors on large areas (as in human skin) is not a problem or hurdle to deal with, but an opportunity to generate power and develop energy autonomous robots. The presented skin possesses additional features such as flexibility, conformability, light weight, robustness, and engineered for specific sensing modality. The demonstrated solar eSkin will potentially open new pathways for power management in robotics.

II. System Overview and Operational Modes

An overview of the design and operation of the solar eSkin system is depicted in the exploded view in Fig. 1, consisting of three main subsystems: 1) power management; 2) sensing; and 3) actuation. The

Manuscript received May 22, 2020; accepted September 3, 2020. Date of publication November 2, 2020; date of current version April 2, 2021. This work was supported by the Engineering and Physical Sciences Research Council (EPSRC) through engineering fellowship for growth under Grant EP/R029644/1 and Grant EP/M002527/1. This article was recommended for publication by Associate Editor J. Paik and Editor E. Yoshida upon evaluation of the reviewers' comments. *(Corresponding author: Ravinder Dahiya.)*

The authors are with the Bendable Electronics and Sensing Technologies (BEST) Group, James Watt School of Engineering, University of Glasgow, G12 8QQ Glasgow, U.K. (e-mail: ravinder.dahiya@glasgow.ac.uk).

This article has supplementary downloadable material available at https://ieeexplore.ieee.org, provided by the authors.
Color versions of one or more of the figures in this article are available online at https://ieeexplore.ieee.org.
Digital Object Identifier 10.1109/TRO.2020.3031264

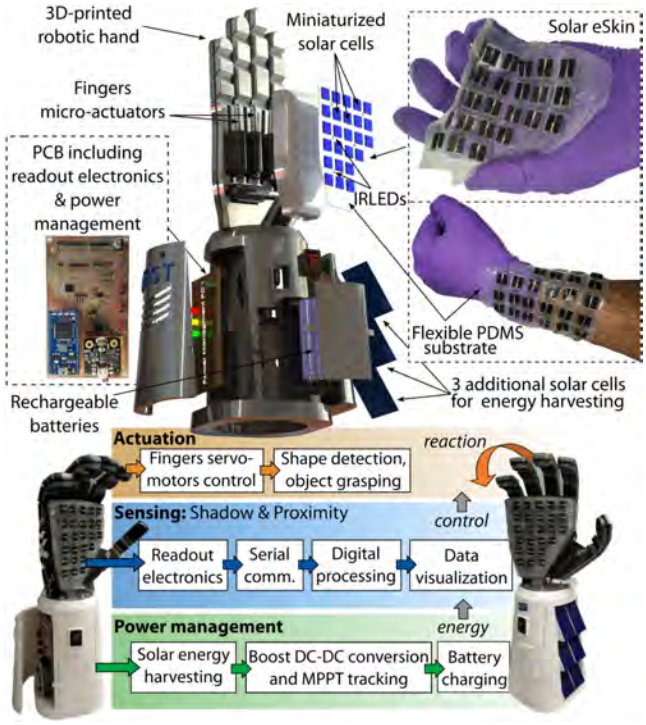

Fig. 1. Overview of the flexible solar eSkin with main components and their integration in the 3-D-printed robotic hand. The block diagram shows the three subsystems: sensing (shadow and proximity modes), power management and actuation.

sensing subsystem consists of a distributed array of miniaturized solar cells and infrared (IR) light emitting diodes (LEDs) integrated on soft and flexible PDMS substrate, which was ultimately placed in the palm of a 3-D-printed robotic hand (Fig. 1). Details regarding the design and fabrication of the 3-D-printed robotic hand can be found in our previous publication [31]. The PDMS film (0.5-mm thickness) was prepared through three stages: 1) mixing of silicone elastomer and curing agent (Sigma Aldrich); 2) degassing; and 3) curing [32], [33]. Before curing, the PV cells were embedded as a matrix over the PDMS layer. By acquiring, combining, and processing the output current of each miniaturized solar cell, it is possible to obtain information for edge detection, shape evaluation, contact location, and proximity detection. To this end, the developed eSkin has two sensing modes: 1) the shadow or darkness sensing mode; and 2) the proximity sensing mode. In both cases, a dedicated circuit instrumentation was developed on a printed circuit board integrated into the robotic wrist as readout for the solar cells array. A serial communication interface was used for sending the real-time measurements to a personal computer (PC) running a custom-developed application, where further processing was conducted prior to the data visualization.

The actuation module, consisting of microlinear actuators controlling the finger movements of robotic hand, is on the top of the sensing subsystem. The processed data coming from the sensing subsystem is used within a control loop to endow the robotic hand with reaction capabilities. This translates into responsive abilities such as detecting location and edges of approaching objects to potentially improve grasping. As previously described, the solar cell array of the eSkin is used both for sensing and energy harvesting. In that way, the power management subsystem (Fig. 1) deals with harvesting and delivery of generated power for the operation of eSkin and, potentially, other devices on the robotic hand. Three additional solar cells were integrated in the robotic wrist to increase the harvested power. Therefore, the functionality of solar cells is further extended beyond their original purpose to achieve a novel paradigm of conformable, energy-surplus solar eSkin.

A. Shadow Sensing

The shadow sensing mode makes use of solar cells in the eSkin in a way that renders solar cells useless with respect to their original purpose, i.e., they do not generate any power when they are covered. By combining the real-time readings of each individual cell in the skin, our system harnesses the information provided by both illuminated and nonilluminated cells to perform the shadow sensing. In that way, the location of approaching objects to the solar skin is achieved along with edge detection, as shown in Fig. 2.

The measured data is transmitted in real-time from the skin to the PC with each cell represented by a color box that changes from green to red depending on the generated output voltage of the cell or, in other words, the level of illumination or shadow that the cell is receiving (*Movie S1* in Supplementary Material). Since the illumination level can vary dynamically depending on the environmental conditions, the shadow sensing and therefore the object detection could be affected. To overcome this limitation, an algorithm was implemented to compute and dynamically update the maximum level of illumination received by each cell. The algorithm takes the first 50 readings from each solar cell and computes the mean, or average, of the values in this set of input data points. While this is done, no object should approach the solar skin. After this, each cell is initiated with the computed averaged value, which corresponds to the mean maximum light that each cell receives under the current ambient light conditions. From there, any object approaching the skin will reduce the amount of light, and, hence, the concept is valid for the sensing purposes. This self-calibration of the colour box representations allows object location and shape detection under different initial lighting conditions. In the demonstration shown in Fig. 2, different objects (a ball and a screwdriver) approach the robotic hand at different locations and orientations and the accompanied graphs show the output voltage of the main cells involved in the object sensing for each of these cases. A real-time representation of the solar skin array (*Movie S2*) shows the object location and their approximate orientation. Considering the data acquisition, communication, and processing times, the sensing delay of the system is $\sim$200 ms. This is approximately the time required to update the visual representation of all cells in the PC application.

Besides the edge detection, Fig. 2 shows that the 3-D shape of the detected object can also be obtained from the solar cells data. To this end, a simple but effective processing was conducted. First, the mean amplitude was obtained for each miniaturized cell in the matrix by averaging the first 50 outputs under normal ambient conditions, i.e., with no object approaching at the time of acquisition. The acquisition of these samples takes less than 2 s and is equivalent to the self-calibration phase previously described. This value is set as the maximum output value for each cell since any object approaching the cells will create a shadow and therefore reduce the output amplitude. Then, the output values of each cell are observed when the object approaches the skin. This corresponds to the moment when the cells under the object are shadowed. The output value of each cell at this time is divided by the maximum value previously acquired during the calibration phase, thus obtaining a normalized value from 0 to 1 for each cell. By representing the calculated matrix of values in a 3-D surface graph (Fig. 2), the 3-D shape of the object face that approaches the skin can be obtained.

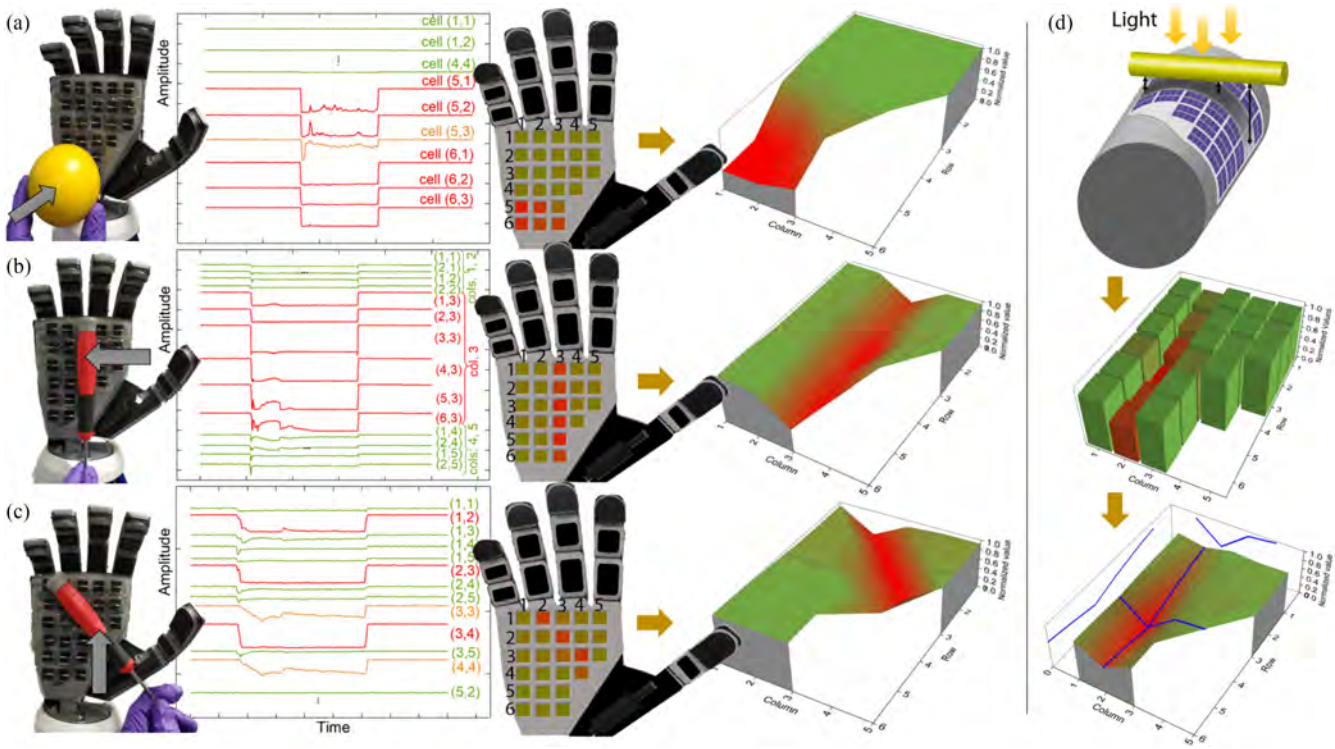

Fig. 2. Shadow sensing mode. (a)–(c). Three examples of contact location, edge detection, and 3-D shape evaluation of different objects approaching toward the eSkin. The graphs in the center show the output voltage of the main cells involved in the object sensing for each case, while the 3-D surface graphs show an evaluation of the reconstructed shape of the object. (d) Simulated scenario in which the skin is attached to a curved surface.

The object shape could be obtained even if the skin was attached to a curved surface such as cylindrical shape as of arm, as shown in Figs. 1 and 2(d). When an object approaches the skin, due to the curvature, the projected shadow will not be uniform over its surface. For example, due to the bending, the shadow will have reduced intensity in the areas farther from the skin. As a result, the output of the shadowed solar cells in the array will not have similar levels. This will result in a nonflat reconstructed shape even if the original object was flat, as shown in Fig. 2(d). Nonetheless, by using the solar cell calibrated output in response to approaching object [Fig. 3(d)], it would be possible to reconstruct the correct image. The eSkin with this conceptual postprocessing and reconstruction will be implemented in future on the curved surfaces. The ability to provide the shape of approaching objects is a distinct feature of presented solar skin, which can be achieved without requiring external power sources. Perhaps, a similar alternative solution could come from a skin based on proximity sensors or the light emitters and detector pair, both of which are power hungry. An array of cameras in eSkin (i.e., skin that can see) could be another potential alternative.

B. Proximity Sensing

The functionality of the solar eSkin was further extended by implementing the proximity sensing mode. In this case, a set of IRLEDs were integrated at the intersection points of the solar cells. Each IRLED was driven by a pulsewidth modulation (PWM) square signal with a frequency of 20 kHz and a duty cycle of 50%. The operation of the proximity sensing mode is based on recording the reflection of IR radiation from the IRLEDs when it bounces off an object approaching the eSkin. The working principle is depicted in Fig 3(a). In summary, the output current is converted to voltage output, after which the offset component of the signal is removed using a dc blocking capacitor. Then, the signal is a sinusoidal waveform whose frequency equals the frequency of the square signal at which the IRLEDs are driven. The amplitude of the signal increases as the object approaches the eSkin, meaning that more radiation is being reflected back to the solar cell. Therefore, the ac signal is rectified and filtered to obtain a constant voltage value at the output of the readout electronics. The resulting signal is then converted to digital domain and digitally filtered for visualization on PC. A demonstration of the proximity sensing mode can be found in *Movies S3* and *S4*. Similar to the shadow sensing mode, the proximity sensing mode could potentially differentiate objects based on basic shapes. In this case, with the additional feature of distance calculation, a robot can potentially sense the existence of an object and pick it up if an appropriate control loop is implemented. A first approach of this concept is shown in *Movie S4*. For a quantitative calibration of the output signal with respect to the distance of approaching object, a custom setup was used. The setup consisted of a square shaped 3×3 cm^2 black plastic probe attached to a controllable linear stage motor, whose vertical movement was precisely controlled in steps of 1 mm through a LabVIEW application [31]. As the probe moved from 26 to 1 mm in the vertical axis, the output of the solar cell (used as proximity sensor) was automatically logged. In this case, the signal amplitude readings were obtained from the solar cell unit (6,1) (see Fig. 2) and the IRLED was placed in the intersection of the four cells in the upper-right corner. Fig. 3(b) shows the temporal response of the system when the probe was moved up and down repeatedly at the maximum speed of the linear actuator (5 mm/s), maintaining the reflecting probe at the closest position for 5 s in each repetition. Similar procedure was followed in Fig. 3(c), but, in this case, the reflecting probe was held in each position for 5 s. In both cases, the acquired raw data is digitally filtered in real

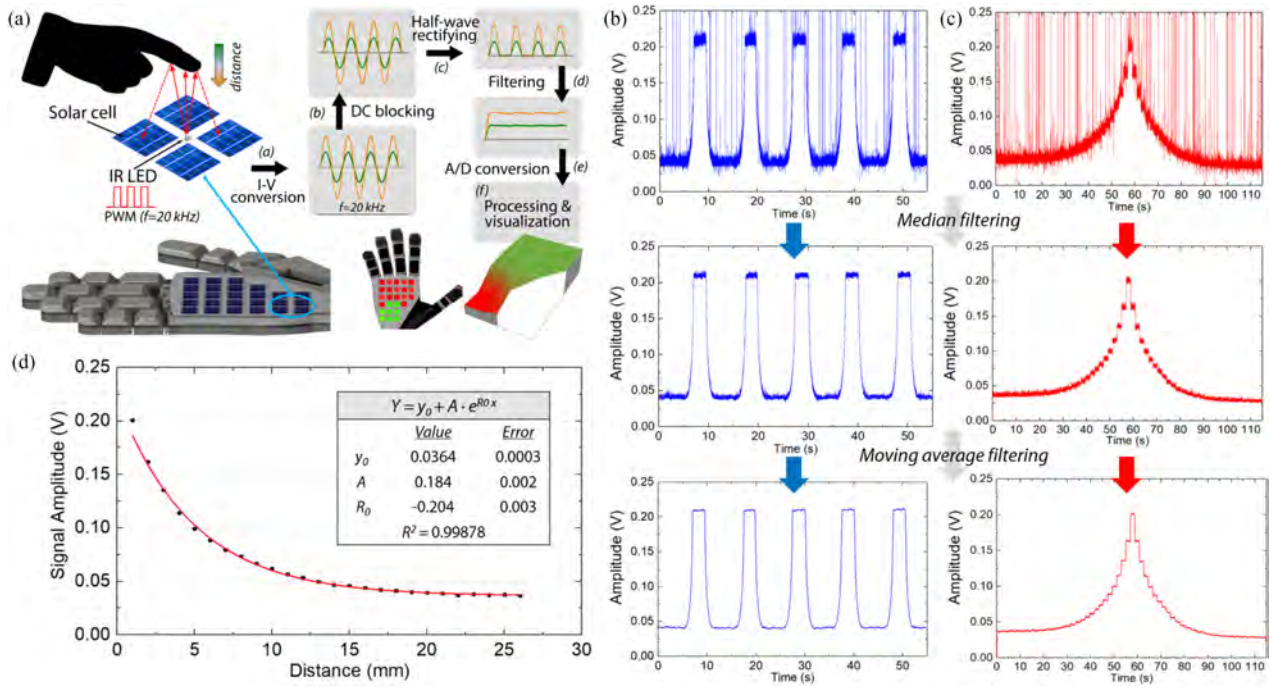

Fig. 3. (a) Proximity sensing mode working principle. (b) and (c) dataflow of signals from the solar eSkin during the proximity sensing characterization. (d) Calibration curve: voltage as a function of distance between the approaching object and the eSkin.

time within a LabVIEW program prior to the visualization. First, the signal is smoothed using a nonlinear median filter with a window rank experimentally set to 2. The filtered data then goes through a moving average filter whose sample length was set to 50 samples. Fig. 3(b) and (c) shows how the noise of the acquired signals is greatly reduced after such processing. A high repeatability of the measurements can be observed from the figure. Fig. 3(d) shows the measured calibration curve of the output voltage as a function of the distance between an approaching object and the skin.

The solar eSkin could potentially provide the robotic hands with tactile feedback for smarter reaction capabilities needed for object grasping and releasing, as well as to ensure safe HRI [34]. As a proof of concept, we have integrated the eSkin on an industrial robot arm UR5 (Universal Robots, Odense, Denmark). Remote control of the UR5 robot was achieved using a client-server model and script commands via TCP socket connection through a custom-developed LabVIEW application. The movements of the UR5 were controlled in response to an object approaching the solar eSkin using the real-time proximity sensing mode. The performance of this system is shown in *Movie S5* (Supplementary Material), where the eSkin detects the approach of a human hand and enables the UR5 robot arm to react immediately by moving away to avoid a collision.

In comparison with the shadow sensing mode, the proximity sensing mode requires more components and a more complex readout circuit. However, it offers interesting features such as the possibility of location recognition and approximate edge detection even in dark environments, i.e., without the need for external light as in the case of shadow sensing.

III. System Design and Performance

At a component level, the solar skin comprises the following blocks:

1) the large area eSkin consisting of the distributed array of miniaturized PV cells and IRLEDs;
2) the power management system;
3) the driver and readout electronics;
4) the digital processing and communication interface.

Fig. 4 shows the block diagram of the complete system and the interconnection between the blocks.

A. Readout Circuit

The heart of the driver and readout electronics is a 32-bit Arm Cortex-M3 microcontroller (MCU) model LPC1768 (NXP Semiconductors, Eindhoven, The Netherlands). This MCU can operate at up to 100 MHz CPU frequencies. It features an USB 2.0 interface, 12-bit analog to digital converter (ADC) with eight channels and conversion rates up to 200 kHz, and 6 PWM outputs. These PWM modules are used to drive the IRLEDs at a fixed frequency of 20 kHz and 50% duty cycle. The LEDs included in the eSkin are IR emitting diodes in gallium-aluminum-arsenides (GaAlAs) multiquantum well technology model TSML1020 (Vishay Semiconductors, Malvern, PA, USA) with peak emission at 940 nm. The output of each PWM module is connected to a silicon *n*-channel MOSFET with low ON-resistance and fast switching speed (model 2SK3541T2L from ROHM Semiconductor, Kyoto, Japan). Each solar cell in the eSkin is connected to an input of a 32-channel analog multiplexer model ADG732 (Analog Devices, Massachusetts, USA), whose output channel is controlled by the MCU. The output of the multiplexer goes through the readout circuit, which varies depending on the selected sensing mode. In the shadow sensing mode, the output of the multiplexer is the input of a current to voltage (*I-V*) converter based on the OPA227 precision bipolar operational amplifier (Texas Instruments, Dallas, TX, USA), which has very low offset voltage (75 μV maximum) and drift. The output of the *I-V* converter is directly connected to an ADC input of the MCU. In the case of the proximity sensing mode, the output of the multiplexer is first filtered using a capacitor to block the dc component. Then an *I-V* converter, with its noninverting input tied to ground, is used. The output of the *I-V* converter goes through a half-wave precision rectifier based on the OPA177 operational amplifier, which features a maximum offset

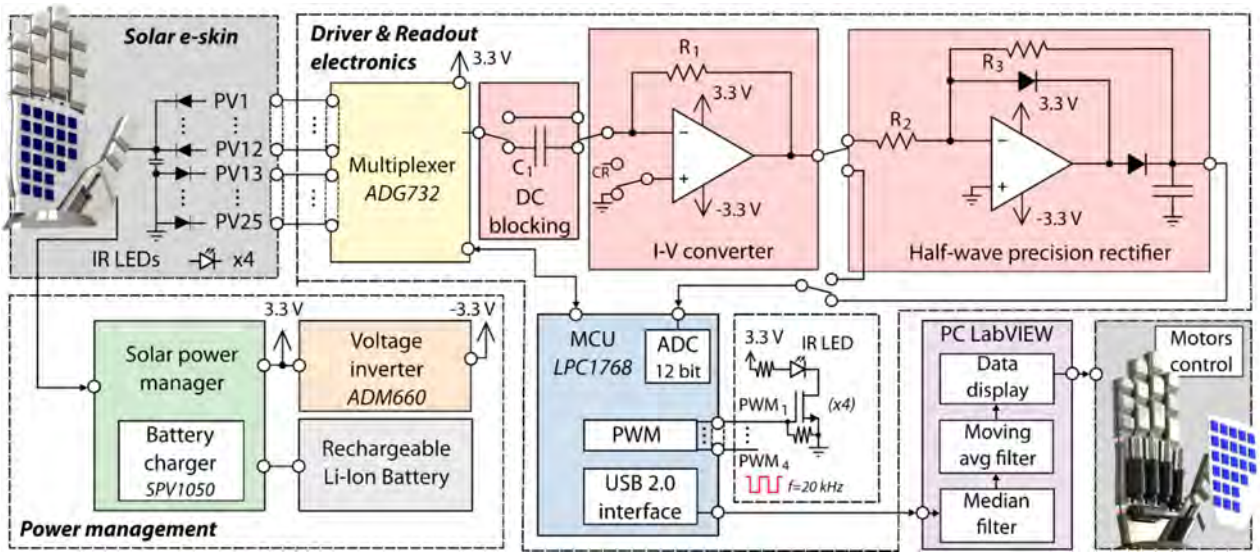

Fig. 4. Schematic block diagram. Schematic diagram showing the main blocks of the developed system: the solar skin as a distributed array of solar cells; the driver and readout electronics; the power management subsystem; and the digital processing and communication interface.

voltage of 25 μV and a low drift of 0.3 μV/°C. Finally, the output of the rectifier is connected to the ADC input of the MCU. By using this configuration, the variations in cells' output current, caused by the reflected radiation from the IRLEDs, are converted to the rectified voltage whose amplitude is related to the distance of the object that reflects the IR radiation (see Fig. 3).

B. Energy Generation and Power Management

The solar cells used in the presented eSkin are commercially available (Pmaxx Series, Silicon Solar, New York, USA) monocrystalline PV cells with an open-circuit voltage (V_{OC}) of 0.55 V and a short-circuit current (I_{SC}) of 100 mA. The purchased cells had an initial size of 7.8 cm^2, but they were cut using a laser engraving machine model Speedy 300 (Trotec Laser, Marchtrenk, Austria) to obtain 1 cm^2 size cells. The resulting small size solar cells were distributed in an array of 25 cells, which was placed as a proof of concept on the palm of the robotic hand. An additional set of three monocrystalline solar panels with $V_{\mathrm{OC}} = 0.5$ V and $I_{\mathrm{SC}} = 850$ mA (model 193852, Sol-Expert group, Baindt, Germany) were placed on the wrist side of the custom-made 3-D-printed hand. These bigger solar cells (50×50 mm^2) could potentially cover a larger surface of the robot's body to further increase the amount of harvested energy. Both models of solar cells were electrically characterized using four-wire measurements with a Precision Source/Measure Unit B2912A (Keysight Technologies, Santa Clara, CA, USA). Fig. 5 shows the electrical characterization of a single miniaturized solar cell in terms of output current I and power P versus output voltage V [35] when illuminated by the light source used in this study. Without illumination, the solar cell has the same electrical characteristics as a diode. When light falls on the cell, the I-V curve shifts as the cell begins to generate power. The greater the light intensity, the greater the amount of shift. The light source is a 4 W LED lamp with color temperature of 4500 K and color rendering index higher than 80 RA (LT-T15, Aglaia, Calabasas, CA, USA). This device generates a white light with an intensity of 650 Lux at a distance of 35 cm. We can identify the open circuit voltage (V_{OC}), the short circuit current (I_{SC}), and the maximum power voltage (V_{MPP}). The output power reaches its peak (P_{MPP}) when the output voltage is at V_{MPP}. Table I shows the measured parameters of each cell derived from their electrical characterizations.

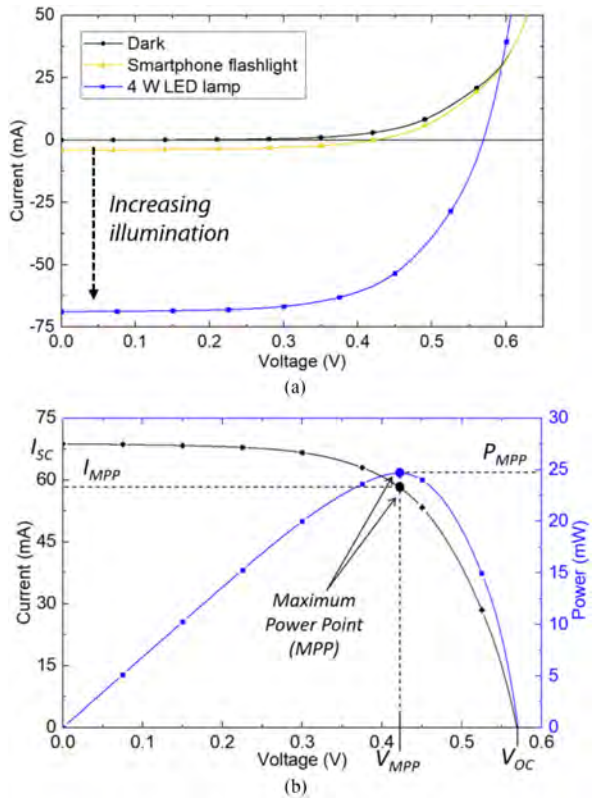

Fig. 5. Electrical characterization of a single PmaxxTM Series solar cell with (a) increasing illumination and (b) light source used in this study, showing, in this case, the I-V and P-V curves and the maximum power point (MPP).

The PV cells in the distributed array are connected in parallel branches. Two types of cells can be differentiated depending on the connection polarity: P-type cells and N-type cells. There are 12 P-type cells (PV1−PV12) whose negative terminals are connected to a common reference (CR) pin, while the rest (PV13−PV25) have their positive terminal connected to the same CR pin. We have designed the circuit to read the change in the illumination with reference to

TABLE I
SOLAR CELLS CHARACTERIZATION

Electrical parameter	Pmaxx solar cell (palm)	193852 solar cell (wrist)
V_{OC}	0.56 V	0.57 V
I_{SC}	68.7 mA	198.1 mA
V_{MPP}	0.43 V	0.39 V
I_{MPP}	57.5 mA	162.8 mA
P_{MPP}	24.7 mW	63.5 mW

that CR pin. So, we can read both the change in the positive direction *P*-type cells and the negative direction *N*-type cells. Since all the cells in the eSkin are connected in parallel branches, one blocking diode or isolation diode has been connected in series to each PV cell to ensure that the electrical current only flows in the desired direction from the array to the external controller. Schottky barrier diodes model UPS115U (Microsemi Corporation, Microchip Technology Inc., Arizona, USA) have been used for this purpose. As opposed to the PN-junction silicon diodes, these Schottky barrier diodes have a much lower voltage drop ($V_f = 220$ mV at 1 A) and allow a more efficient scheme with less power dissipation in each blocking diode.

The output of the array of PV cells is connected to a micropower, high-efficiency solar power management module ISV019V1 (STMicroelectronics, Geneva, Switzerland), which is based on the SPV1050 integrated circuit. The SPV1050 is an ultra-low power energy harvester with an embedded maximum power point tracking (MPPT) algorithm, a battery charger, and a power manager. It integrates a dc−dc converter stage that has been configured as boost, providing a regulated output voltage of 3.3 V. By enabling the MPPT feature, the SPV1050 regulates the working point of the dc−dc converter by tracking its output voltage so that $V_{\mathrm{IN}} = V_{\mathrm{MPP}}$, thus maximizing the power extracted from the source [36]. In fact, V_{MPP} is a fraction of the open circuit voltage V_{OC} of the harvesting source. Although P_{MPP} increases with illumination, the V_{MPP} changes little. Therefore, we may approximately take the V_{MPP} as a constant for a specific solar cell under different illuminations. This value is usually 70−80% of the V_{OC} voltage. The SPV1050 chip used in this module uses a constant voltage ratio MPPT algorithm to control the output voltage of the solar panel about 75% of the open circuit voltage to maximize the output power of the solar panel. Using the ISV019V1 module, we are able to charge a 3.7 V Li-Po battery through solar energy harvesting with a charge current up to 70 mA. The integrated boost dc−dc converter starts working from an input voltage as low as 150 mV and is able to provide up to 200 mA at 3.3 V, i.e., 660 mW. In our case, the driver and readout electronics consumption are 23.9 mA at 3.3 V (78.9 mW) without considering the MCU. In active mode and at the maximum operating frequency of 100 MHz, the LPC1768 MCU consumes a total power of 155 mW (47 mA at 3.3 V), considering not only the power consumption of the MCU but also the consumption of all used peripherals [universal asynchronous receiver/transmitter (UART), PWM, and ADC modules]. This power consumption can be further reduced if a lower clock frequency is selected (e.g., 12 MHz) at the expense of a slower system operation.

Thanks to the MPPT feature of the solar power manager, we can consider that the cells will be working close to the maximum power point (MPP) under adequate light conditions. If all cells in the palm of the robotic hand were working on the MPP measured with the light source used in this study, the presented skin would generate more than twice the power required for the system operation in active mode at the highest clock rate of 100 MHz (Table II). If we include the additional array of solar cells placed in the wrist, the harvested power is more than

TABLE II
POWER BUDGET: SUMMARY OF THE SURPLUS POWER GENERATED AFTER CONSIDERING GENERATION AND CONSUMPTION OF THE SOLAR ESKIN

System	Conditions	Surplus Power (mW)
Complete solar eSkin powered by palm solar cells	100 MHz, all palm cells at MPP	383.6
	100 MHz, 40% of palm cells at MPP	13.10
	12 MHz, all palm cells at MPP	501.7
	12 MHz, 40% of palm cells at MPP	131.2
	12 MHz, 30% of palm cells at MPP	69.50
Complete solar eSkin system powered by palm and wrist solar cells	100 MHz mode, all cells at MPP	574.1
	100 MHz mode, 40% cells at MPP	89.30
	100 MHz mode, 30% cells at MPP	8.50
	12 MHz mode, all cells at MPP	692.2
	12 MHz mode, 40% cells at MPP	207.4
	12 MHz mode, 30% cells at MPP	126.6
	12 MHz mode, 15% cells at MPP	5.40

three times the required power for the system operation. However, it is unrealistic to think that the system will always operate under these ideal conditions, i.e., all the cells will be illuminated all the time to allow the maximum power generation. Considering the maximum required power (233.9 mW), we would be able to operate the system using 40% of the solar cells in the palm of the robotic hand working at the MPP. When adding the power harvested by the wrist solar cells, this percentage can be reduced down to 30%. In any case, the surplus energy generated under adequate light conditions could be used to charge the battery through the solar power management module based on the SPV1050 chip. Table II shows the net surplus power generated after considering generation and consumption under different conditions. Considering that our flexible eSkin has a total palm area of 55.5 cm^2, with a net gain of 383.6 mW from the palm area only (active mode at 100 MHz and all the palm cells working at MPP), the solar eSkin over the whole body would generate more than 100 W. This value has been estimated considering a robotic body area equivalent to human skin (i.e., 1.5 m^2). In the case of a more realistic situation where not all the cells are working at MPP, but 40% of them are, the solar eSkin over the whole body would still generate around 35 W. This level of energy generated by the eSkin is good enough to drive other devices (e.g., actuators, external sensors etc.) in a robotic hand.

Moreover, a more efficient usage of the energy can be achieved by implementing an event-driven strategy in the MCU [20], [21], given that its power consumption in sleep mode is only 6.6 mW. The peripheral functions continue operation during sleep mode and may generate interruptions to cause the processor to resume execution. In the event-driven approach, the MCU spends the majority of the time in sleep mode until the moment an external level sensitive interruption is triggered, i.e., an object approaches the solar skin, thus increasing the input voltage of the ADC above a predefined threshold. In that moment, the MCU wakes up to the active mode, where the sensing acquisition is continuous. When sufficient time goes by without detecting the presence of an object, the MCU goes back to sleep mode waiting for the next triggering event. In that case, the battery life is further enhanced as the solar cells are continuously charging the battery at a higher rate than the demands from the readout circuit.

IV. CONCLUSION

In this article, the operating principle of solar cells was harnessed for touch sensing, and, thus, the solar cells were used as energy harvesters and touch sensors at the same time. Based on this approach, a large area flexible and conformable eSkin was developed by distributing miniaturized solar cells in a matrix. As a proof of concept, the developed

solar eSkin was integrated into a custom-designed 3-D-printed robotic hand which includes microlinear servomotors for controlling the actuation of the fingers. In the first approach, the solar cells in the matrix was used as darkness/shadow detectors, and, thus, these electrical devices were exploited even when they are supposed to be useless (i.e., not generating energy). The combined output of all the illuminated and, more importantly, nonilluminated solar cells in the matrix allows us to conduct sensing measurements such as object location, edge detection, and shape evaluation. Further, the solar eSkin was used not only as shadow or darkness detector but also for proximity sensing. By adding a number of IRLEDs and a smarter readout circuit to the solar eSkin, the proximity sensing mode is able to quantify the close proximity of objects approaching to the robotic hand. The proximity sensing mode allows the robot to operate in dark environments, as the light source for the sensing relies on the IRLEDs included in the eSkin. These are significant advances while generating net positive energy. Under adequate light conditions, the readout electronics used for the sensing operation is directly powered by the energy generated by the solar eSkin itself, thus becoming an energy autonomous system as a whole. In fact, the surplus of energy can be stored in the batteries as a backup for later use when the light conditions are not good enough to generate the required power. A further step has been taken by integrating the 3-D-printed hand with solar eSkin onto an industrial robot arm UR5 from Universal Robots. The real-time closed control loop implemented to endow the robot arm with reaction capability shows the eSkin operating effectively in proximity sensing mode to prevent collisions of robotic hand with approaching objects or individuals, thus opening a promising route for safe HRI.

Unlike centralized basic sensory modalities (e.g., vision, audio, etc.), the tactile skin is distributed over the whole body along with the sensors embedded in it. The large area distribution of sensors in the tactile skin is often said to be a major challenge for development and effective use of skin in robotics. Among various challenges (e.g., data handling, routing of wires, etc.), the growing energy requirements of distributed sensors is also a major issue which has not received much attention so far. While addressing the energy-related challenge, the work presented in this article also showed that the presence of skin on large area is not a challenge, instead it is an opportunity. For example, with a net energy surplus of 383.6 mW from the palm area of a robotic hand only, the presented eSkin over and area of $\sim$1.5 m^2 (approximately the area of skin in humans) would generate more than 100 W, which is sufficient to operate several other devices including the actuators in the hand.

It is also worth mentioning the potential limitations of presented eSkin so as to drive the improvement in the future. First, the flexibility of the presented eSkin could be limited by the use of miniaturized but rigid solar cells. The current version of eSkin can be bent easily without breaking to conform to curved cylindrical surfaces with radius of curvature as low as 30 mm, as in the arms or a wrist. This is already better than the flexible printed circuits based large areas skins reported in the literature [21], [26], [37], [38] but still insufficient if the body parts such as fingers are to be covered. The ultra-bendability could be achieved either by further miniaturization of rigid solar cells or by using flexible solar cells [39], [40]. Furthermore, energy storage devices such as flexible supercapacitors could be added to solar cells to store energy for later use when there is no light [29], [41].

Another limitation can arise during scenarios where the light conditions change drastically, or when the light source is not stationary. In such cases, the implemented sensing algorithms could result in false or incorrect detections. Some mitigation of these effects can be achieved by frequently running the "self-calibration" algorithm described in Section II. For example, during moving light source, the variation of light on various cells will be same. This means the relative variation among solar cells will be negligible, and, hence, the eSkin will work normally. However, this may change in the presence of multiple moving light sources. Further processing of the output data of the eSkin could also help in this type of complex scenarios.

In summary, in this article, the functionality of solar cells was extended beyond their original purpose to develop a novel paradigm for flexible, conformable, energy-surplus solar eSkin that is integrated into a robotic hand to endow it with reaction capabilities for HRI applications. Future work will explore the extension of the solar eSkin for shadow and proximity sensing to other body parts of a robot such as the arm or the chest. In such scenarios, the proposed system would be useful for improved safety and security for human−robot coexistence and for continuous operation of actuators in the hand or other parts of robot.

REFERENCES

[1] R. Dahiya, "E-Skin: From humanoids to humans [point of view]," *Proc. IEEE*, vol. 107, no. 2, pp. 247–252, Feb. 2019.

[2] T. Belpaeme, J. Kennedy, A. Ramachandran, B. Scassellati, and F. Tanaka, "Social robots for education: A review," *Sci. Robot.*, vol. 3, no. 21, 2018, Art. no. eaat5954.

[3] I. Leite, C. Martinho, and A. Paiva, "Social robots for long-term interaction: A survey," *Int. J. Soc. Robot.*, vol. 5, no. 2, pp. 291–308, 2013.

[4] R. S. Dahiya and M. Valle, *Robotic Tactile Sensing: Technologies and System*. Berlin, Germany: Springer, 2013.

[5] B. D. Argall and A. G. Billard, "A survey of tactile human–robot interactions," *Rob. Auton. Syst.*, vol. 58, no. 10, pp. 1159–1176, 2010.

[6] T. Yamaguchi, T. Kashiwagi, T. Arie, S. Akita, and K. Takei, "Human-like electronic skin-integrated soft robotic hand," *Adv. Intell. Syst.*, vol. 1, no. 2, 2019, Art. no. 1900018.

[7] Y. Lee, J. Park, A. Choe, S. Cho, J. Kim, and H. Ko, "Mimicking human and biological skins for multifunctional skin electronics," *Adv. Funct. Mater.*, vol. 1904523, 2019, Art. no. 1904523.

[8] M. Xie *et al.*, "Flexible multifunctional sensors for wearable and robotic applications," *Adv. Mater. Technol.*, vol. 4, no. 3, pp. 1–29, 2019.

[9] H. He *et al.*, "A self-powered electronic-skin for real-time perspiration analysis and application in motion state monitoring," *J. Mater. Chem. C*, vol. 6, no. 36, pp. 9624–9630, 2018.

[10] C. Zhang, S. Liu, X. Huang, W. Guo, Y. Li, and H. Wu, "A stretchable dual-mode sensor array for multifunctional robotic electronic skin," *Nano Energy*, vol. 62, pp. 164–170, 2019.

[11] R. Dahiya *et al.*, "Large-area soft e-skin: The challenges beyond sensor designs," *Proc. IEEE*, vol. 107, no. 10, pp. 2016–2033, Oct. 2019.

[12] S. Baek *et al.*, "Flexible piezocapacitive sensors based on wrinkled microstructures: Toward low-cost fabrication of pressure sensors over large areas," *RSC Adv.*, vol. 7, no. 63, pp. 39420–39426, 2017.

[13] M. Bhattacharjee, M. Soni, P. Escobedo, and R. Dahiya, "PEDOT:PSS microchannel-based highly sensitive stretchable strain sensor," *Adv. Electron. Mater.*, vol. 6, no. 8, 2020, Art. no. 2000445.

[14] R. D. I. G. Dharmasena *et al.*, "Energy scavenging and powering E-Skin functional devices," *Proc. IEEE*, vol. 107, no. 10, pp. 2118–2136, Oct. 2019.

[15] C. García Núñez, L. Manjakkal, and R. Dahiya, "Energy autonomous electronic skin," *NPJ Flex. Electron.*, vol. 3, no. 1, 2019, Art. no. 1.

[16] L. Manjakkal, C. G. Núñez, W. Dang, and R. Dahiya, "Flexible self-charging supercapacitor based on graphene-Ag-3D graphene foam electrodes," *Nano Energy*, vol. 51, pp. 604–612, Sep. 2018.

[17] D.-H. Kim *et al.*, "Epidermal electronics," *Science*, vol. 333, no. 6044, pp. 838–843, 2011.

[18] C. Jiang, H. W. Choi, X. Cheng, H. Ma, D. Hasko, and A. Nathan, "Printed subthreshold organic transistors operating at high gain and ultralow power," *Science*, vol. 363, no. 6428, pp. 719–723, 2019.

[19] C. Jiang, X. Cheng, and A. Nathan, "Flexible ultralow-power sensor interfaces for E-Skin," *Proc. IEEE*, vol. 107, no. 10, pp. 2084–2105, Oct. 2019.

[20] G. Cheng, E. Dean-Leon, F. Bergner, J. Rogelio Guadarrama Olvera, Q. Leboutet, and P. Mittendorfer, "A comprehensive realization of robot skin: Sensors, sensing, control, and applications," *Proc. IEEE*, vol. 107, no. 10, pp. 2034–2051, Oct. 2019.

[21] R. S. Dahiya, P. Mittendorfer, M. Valle, G. Cheng, and V. J. Lumelsky, "Directions toward effective utilization of tactile skin: A review," *IEEE Sens. J.*, vol. 13, no. 11, pp. 4121–4138, Nov. 2013.
[22] W. W. Lee *et al.*, "A neuro-inspired artificial peripheral nervous system for scalable electronic skins," *Sci. Robot.*, vol. 4, no. 32, 2019, Art. no. eaax2198.
[23] Y. Wu *et al.*, "A skin-inspired tactile sensor for smart prosthetics," *Sci. Robot.*, vol. 3, no. 22, pp. 1–9, 2018.
[24] L. E. Osborn *et al.*, "Prosthesis with neuromorphic multilayered e-dermis perceives touch and pain," *Sci. Robot.*, vol. 3, no. 19, 2018, Art. no. eaat3818.
[25] R. Dahiya, D. Akinwande, and J. S. Chang, "Flexible electronic skin: From humanoids to humans [scanning the issue]," *Proc. IEEE*, vol. 107, no. 10, pp. 2011–2015, Oct. 2019.
[26] K. Yu, S. Rich, S. Lee, K. Fukuda, T. Yokota, and T. Someya, "Organic photovoltaics: Toward self-powered wearable electronics," *Proc. IEEE*, vol. 107, no. 10, pp. 2137–2154, Oct. 2019.
[27] G. Min, L. Manjakkal, D. M. Mulvihill, and R. S. Dahiya, "Triboelectric nanogenerator with enhanced performance via an optimized low permittivity substrate," *IEEE Sens. J.*, vol. 20, no. 13, pp. 6865–68621, Jul. 2019.
[28] C. G. Núñez, W. T. Navaraj, E. O. Polat, and R. Dahiya, "Energy-autonomous, flexible, and transparent tactile skin," *Adv. Funct. Mater.*, vol. 27, no. 18, 2017, Art. no. 1606287.
[29] L. Manjakkal, W. T. Navaraj, C. G. Núñez, and R. Dahiya, "Graphene–graphite polyurethane composite based high-energy density flexible supercapacitors," *Adv. Sci.*, vol. 6, no. 7, 2019, Art. no. 1802251.
[30] W. K. Chee, H. N. Lim, Z. Zainal, N. M. Huang, I. Harrison, and Y. Andou, "Flexible graphene-based supercapacitors: A review," *J. Phys. Chem. C*, vol. 120, no. 8, pp. 4153–4172, 2016.
[31] M. Ntagios, H. Nassar, A. Pullanchiyodan, W. T. Navaraj, and R. Dahiya, "Robotic hands with intrinsic tactile sensing via 3D printed soft pressure sensors," *Adv. Intell. Syst.*, vol. 2, 2019, Art. no. 1900080.
[32] S. Gupta, A. Vilouras, and R. Dahiya, "Polydimethylsiloxane as polymeric protective coating for fabrication of ultra-thin chips," *Microelectron. Eng.*, vol. 301, 2019, Art. no. 111157.
[33] R. Dahiya, G. Gottardi, and N. Laidani, "PDMS residues-free micro/macrostructures on flexible substrates," *Microelectron. Eng.*, vol. 136, pp. 57–62, 2015.
[34] P. A. Lasota, T. Fong, and J. A. Shah, "A survey of methods for safe human-robot interaction," *Found. Trends Robot.*, vol. 5, no. 3, pp. 261–349, 2017.
[35] P. Escobedo, I. M. P. de Vargas-Sansalvador, M. Carvajal, L. F. Capitán-Vallvey, A. J. Palma, and A. Martínez-Olmos, "Flexible passive tag based on light energy harvesting for gas threshold determination in sealed environments," *Sens. Actuators B Chem.*, vol. 236, pp. 226–232, 2016.
[36] A. D. Grasso, G. Palumbo, and S. Pennisi, "Switched-capacitor power management integrated circuit for autonomous internet of things node," *IEEE Trans. Circuits Syst. II Express Briefs*, vol. 65, no. 10, pp. 1455–1459, Oct. 2018.
[37] R. Dahiya, W. T. Navaraj, S. Khan, and E. O. Polat, "Developing electronic skin with the sense of touch," *Inf. Disp. 1975*, vol. 31, no. 4, pp. 6–10, 2015.
[38] A. Schmitz, P. Maiolino, M. Maggiali, L. Natale, G. Cannata, and G. Metta, "Methods and technologies for the implementation of large-scale robot tactile sensors," *IEEE Trans. Robot.*, vol. 27, no. 3, pp. 389–400, Jun. 2011.
[39] K.-J. Yang *et al.*, "Flexible Cu2ZnSn(S,Se)4 solar cells with over 10% efficiency and methods of enlarging the cell area," *Nat. Commun.*, vol. 10, no. 1, 2019, Art. no. 2959.
[40] S. A. Hashemi, S. Ramakrishna, and A. G. Aberle, "Recent progress in flexible–wearable solar cells for self-powered electronic devices," *Energy Environ. Sci.*, vol. 13, no. 3, pp. 685–743, 2020.
[41] L. Manjakkal, A. Pullanchiyodan, N. Yogeswaran, E. S. Hosseini, and R. Dahiya, "A wearable supercapacitor based on conductive PEDOT:PSS-coated cloth and a sweat electrolyte," *Adv. Mater.*, 2020, Art. no. 1907254.